SUPPLEMENTARY FIGURES

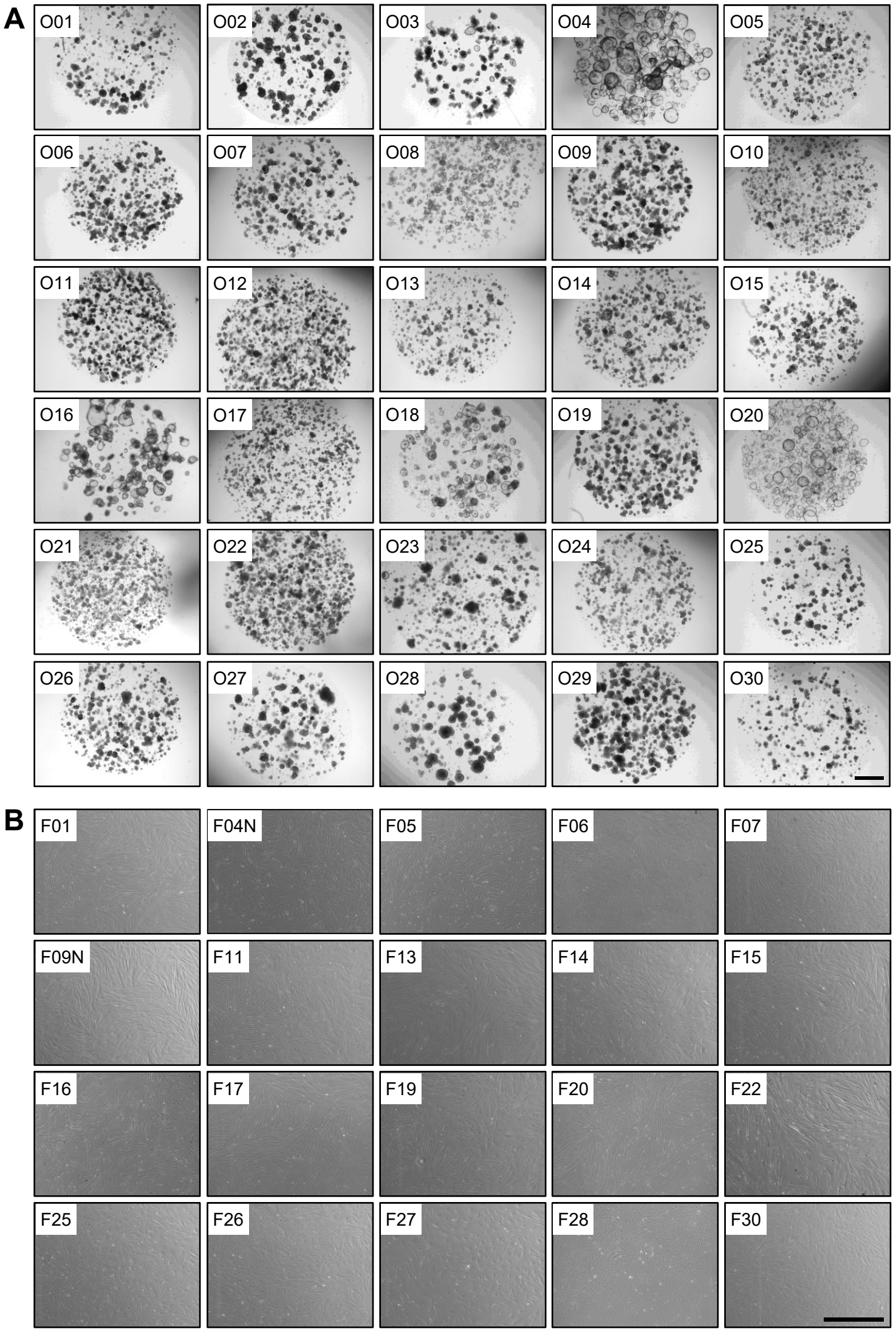

Supplementary Figure S1 | CRC organoid and fibroblast morphology.
A) Morphological overview of organoids derived from different patients. All images were captured using a 2× objective magnification. Scalebar is 1 mm.
B) Primary fibroblasts grown in adhesive culture. Phase contrast images captured using a 4× objective. F04N and F09N are fibroblasts derived from normal tumor-adjacent mucosa. Scalebar is 1 mm.

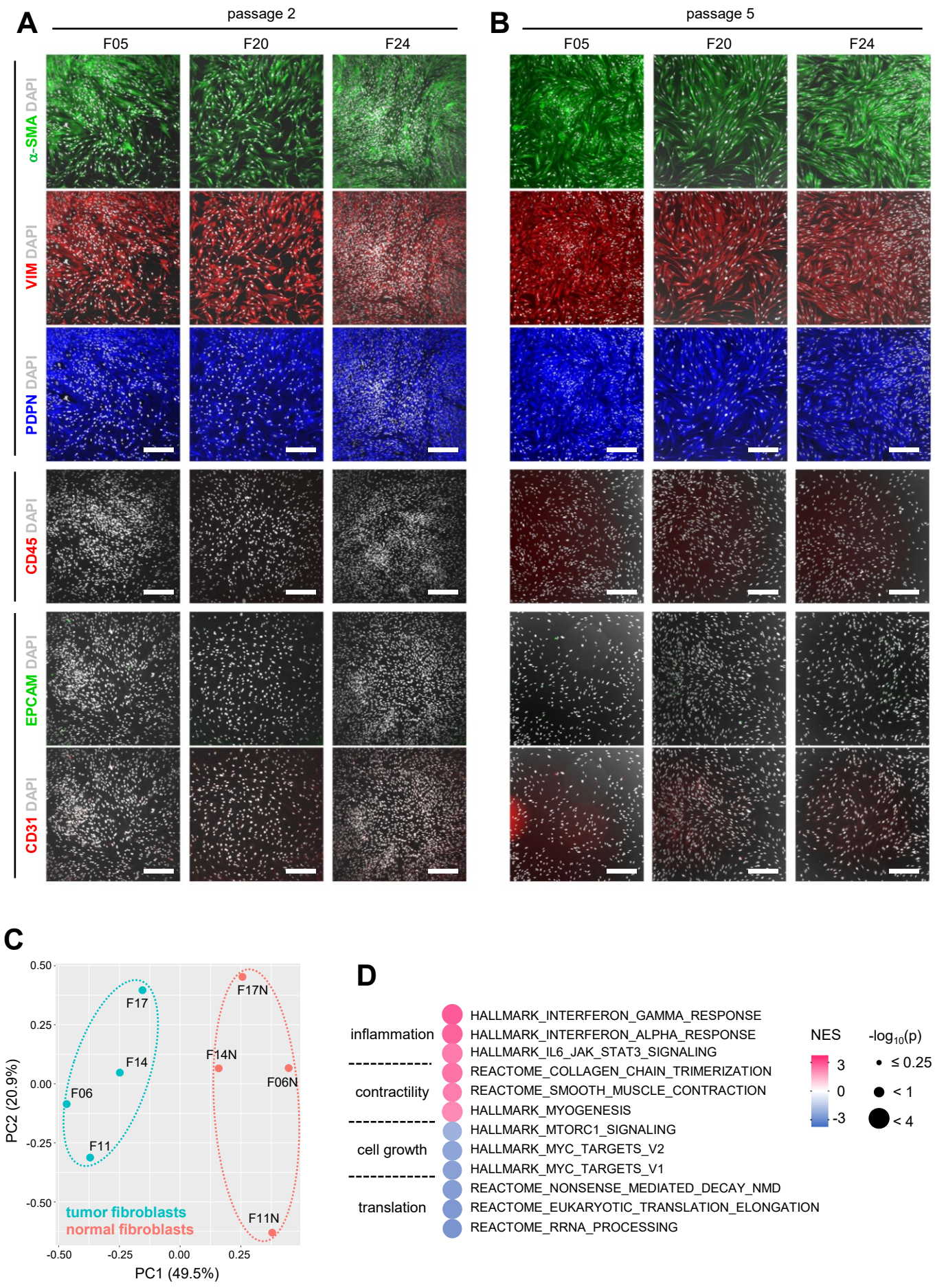

Supplementary Figure S2 | Characterization of CAFs after *in vitro* culture.
A-B) Immunofluorescent analysis of tumor fibroblasts early after isolation (passage 2; A) and after prolonged culture (passage 5; B). Cells from three individuals were cultured as indicated in the methods section. Staining of fibroblast markers α-SMA, VIM and PDPN shows stable and homogenous phenotype *in vitro*. Markers for immune cells (CD45), epithelial cells (EPCAM) and endothelial cells (CD31) were stained to determine purity. Nuclei were stained with DAPI. All scale bars are 300 µm.
C-D) RNA sequencing of matched normal and tumor fibroblasts (n=4). All cells were cultured for at least 5 passages. C) Principal component analysis shows differences among tumor and normal fibroblasts. D) GSEA of differentially expressed MSigDB signatures in normal and tumor fibroblasts (paired analysis). The most prominently enriched signatures in tumor fibroblasts are associated with inflammation and cell contractility. Cell growth and translation signatures are increased in normal fibroblasts. NES and p-values are shown.

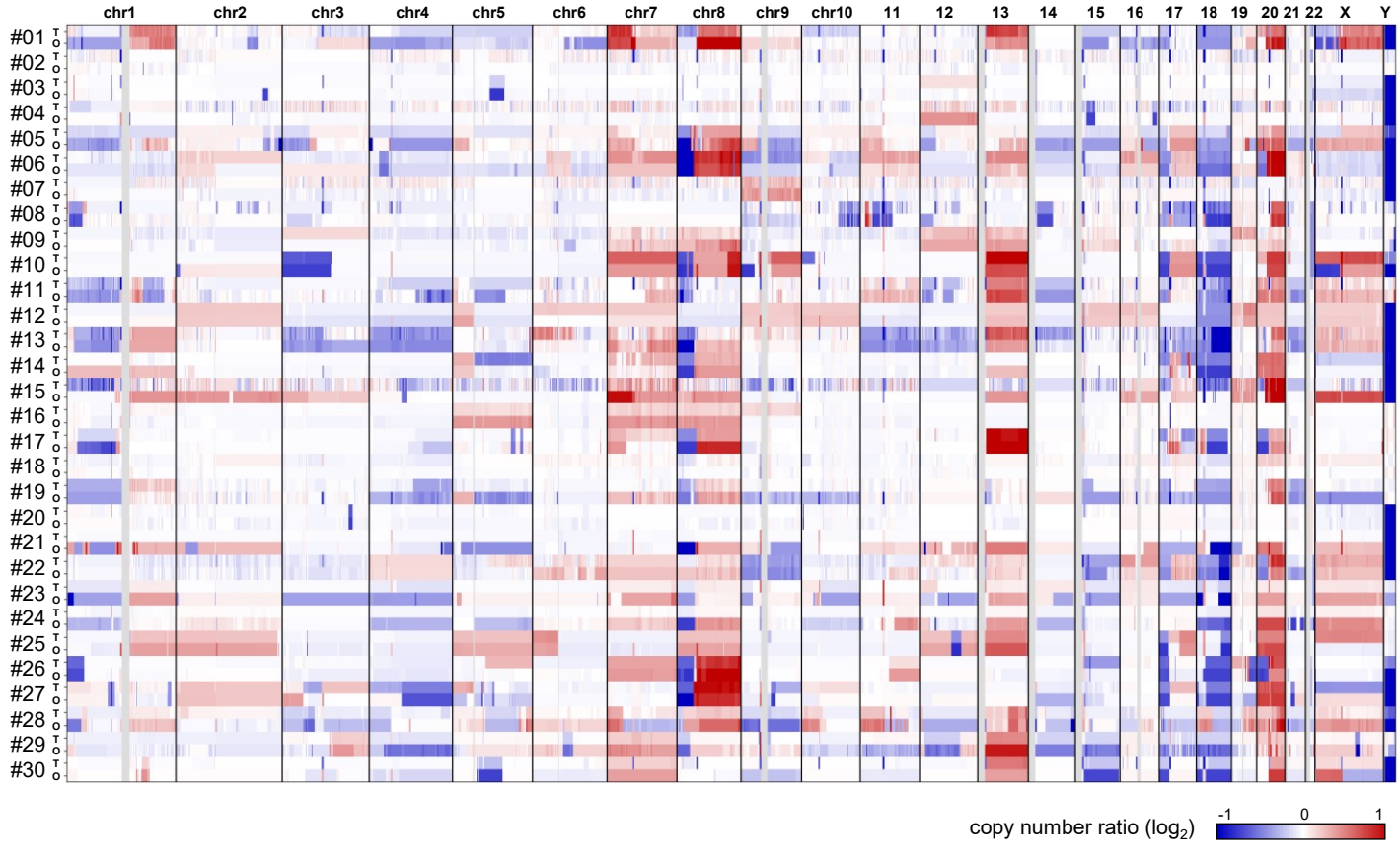

Supplementary Figure S3 | CNV analysis.
Heatmap of copy number ratios determined from exome sequencing data. For each model (#01-#30) CNVs in tumors (T) and organoids (O) is shown.

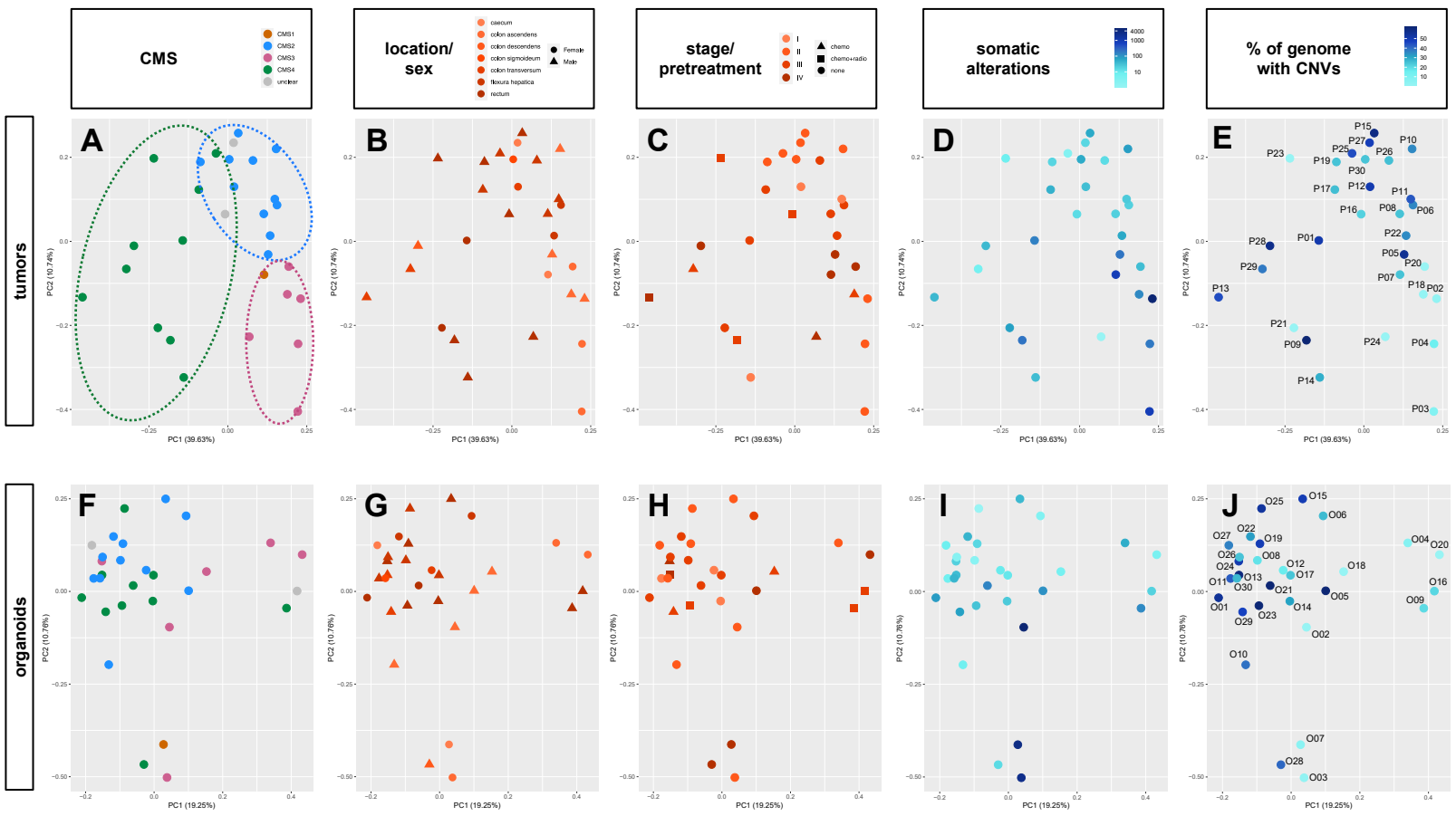

Supplementary Figure S4 | Principal component analysis of transcriptomic data in relation to clinical and pathological features.
RNA sequencing data from original tumors (T01-T30; A-E) and organoids (O01-O30; F-J). Note that the CMS represents the main source of variability in original tumors (A, colored ellipsoids) but not in corresponding organoids (F) where the CMS of the original tumors is marked. Tumor location and patient sex (B, G), tumor stage and radio-/chemotherapy pretreatment (C, H), number of somatic alterations in tumors (D) and organoids (I), and percentage of genome with CNVs in tumors (E) and organoids (J) are shown. ID numbers of each sample are given in (E, J).

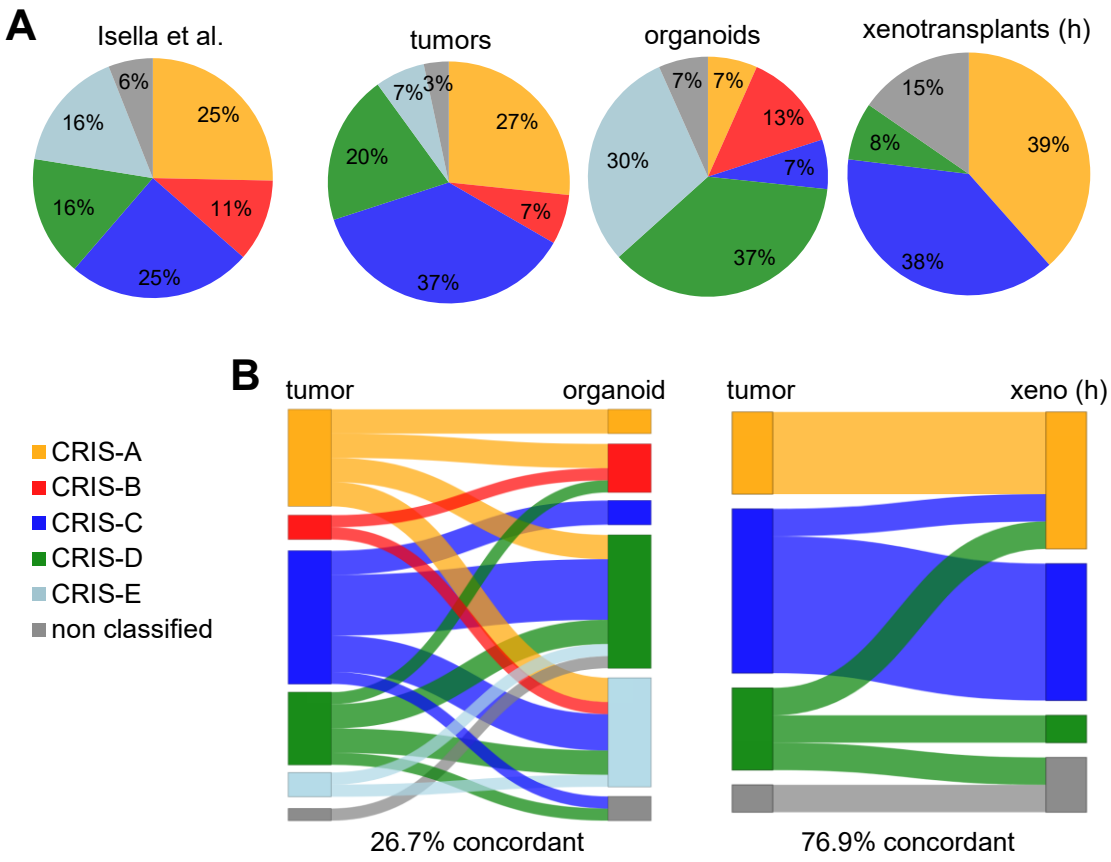

Figure S5 | The cancer intrinsic subtypes (CRIS) depend on the microenvironmental context.
A) CRIS classification (performed as described in methods). Pie charts show public data from Isella et al., 2017 (8) using the TCGA cohort ([28]), 450 samples) and classification of organoid-stroma biobank. Tumors, matched organoids (n=30) and subcutaneous PDTO transplantation in *NSG* mice. An arbitrary subset of xenotransplants (n=13) was analyzed by RNA sequencing and human reads (h) were studied. For information on xenotransplant growth see Supplementary Table S2.
B) Sankey plots show weak overlap between tumors and organoids and improved concordance to the CRIS in corresponding tumors after xenotransplantation.
See Supplementary Table S6.

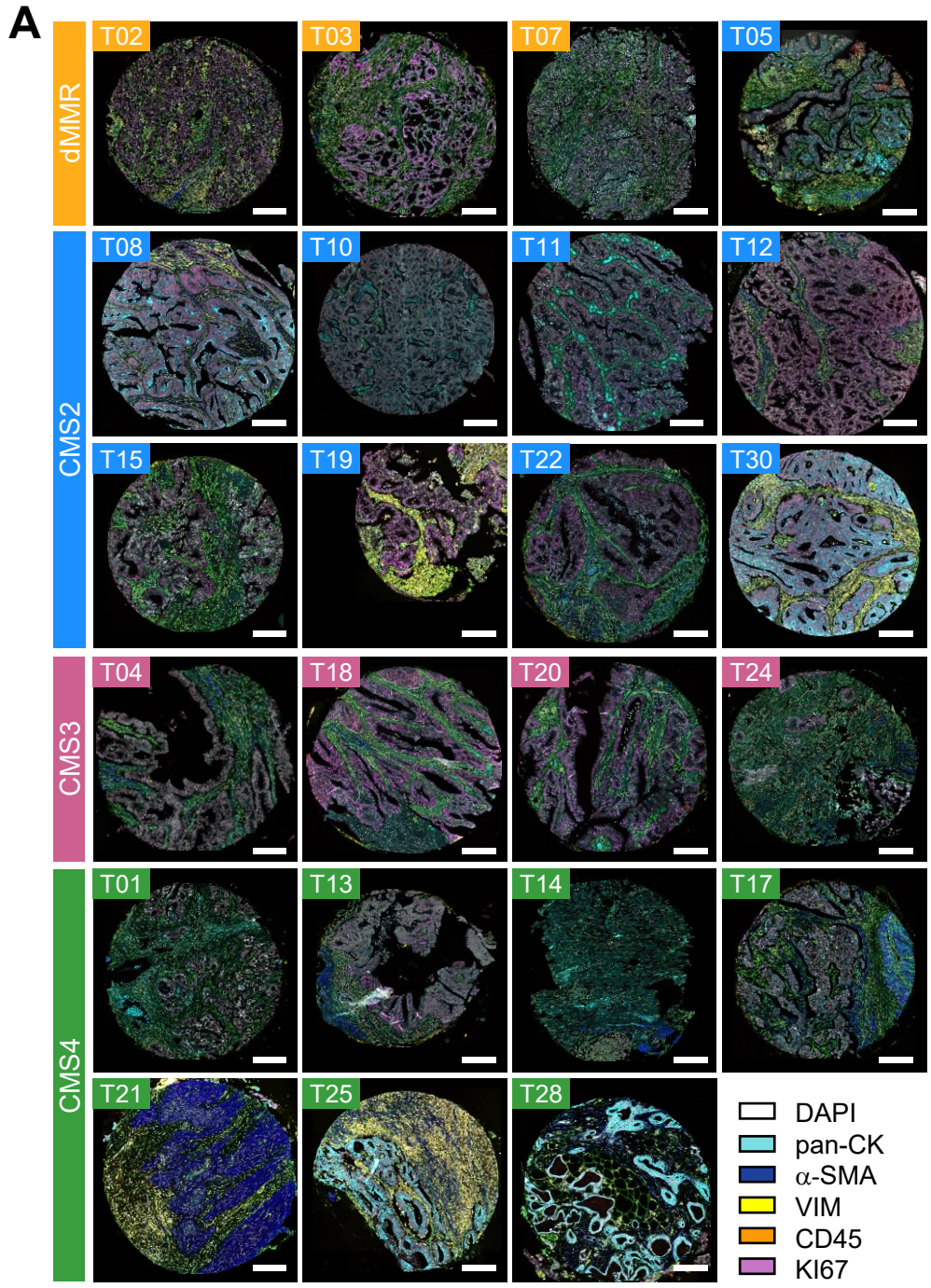

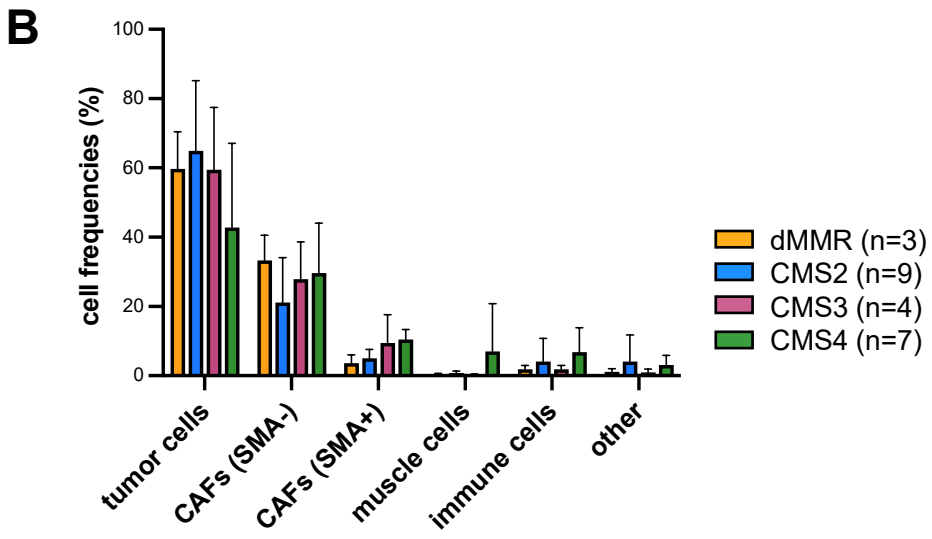

Supplementary Figure S6 | Multiplex immunofluorescence staining of tissue microarray (TMA) from CRC samples.

A) Overview images of TMA stained by multiplex immunofluorescence to characterize the tumor microenvironment. Scale bars are 200 µm.

B) Summary of cell frequencies (mean ±SD) in the different subtypes. Cell types were automatically assigned by the phenotype functionality of the inForm software. VIM^+ CAFs were distinguished into α-SMA^+ or α-SMA^- cells. Immune cells were detected by CD45 staining. Non-classified cells were listed under the category 'other'.

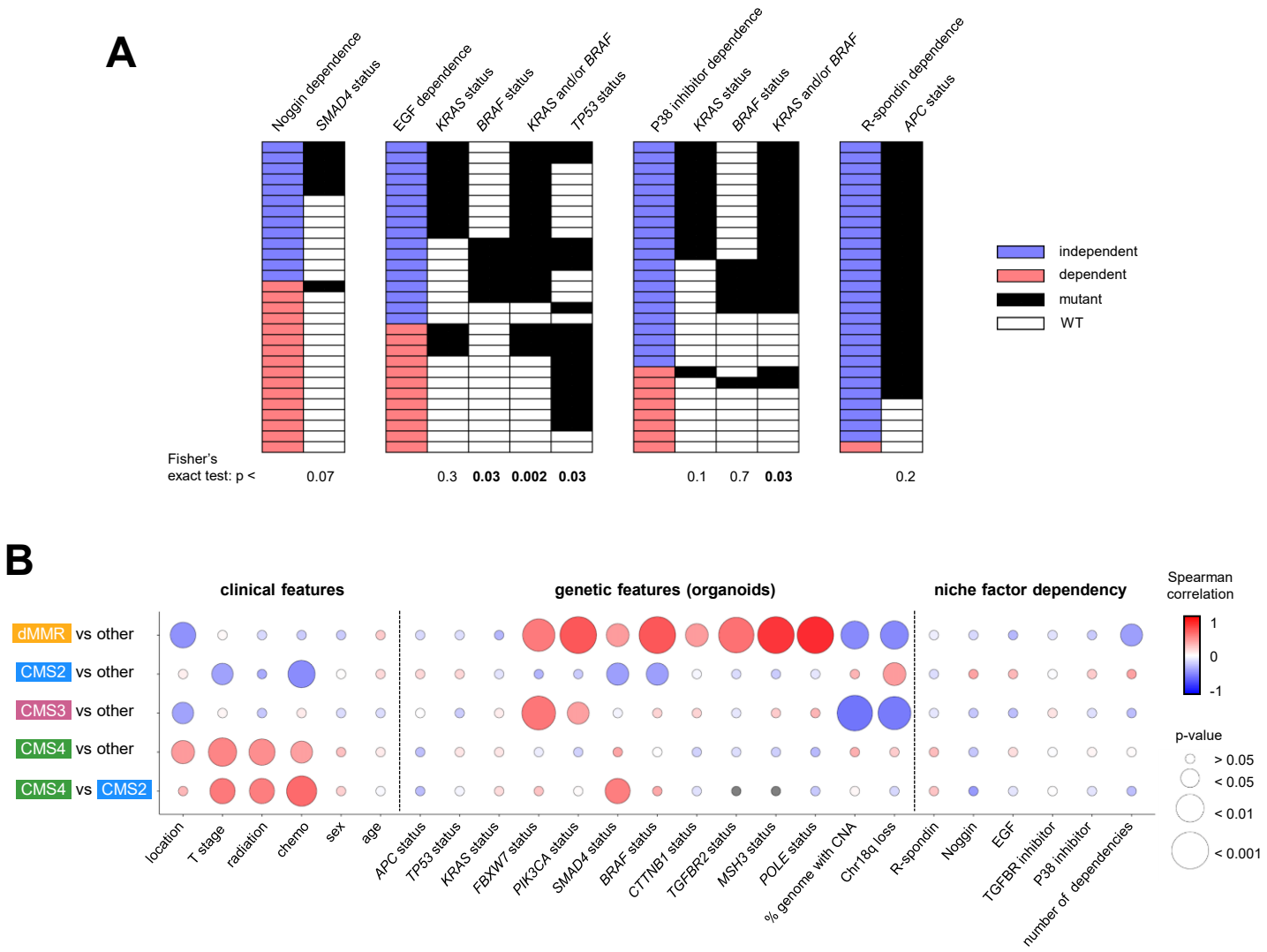

Supplementary Figure S7 | Tumor organoid niche factor dependency and association with genetic, clinical and transcriptomic features.

A) Comparison of niche factor requirements (n=29) with identified tumor mutations (VAF >5% in PDTOs). Dependence of Noggin, EGF, p38 inhibitor and R-spondin is shown. Statistical significance was studied by Fischer's exact test or Mann-Whitney-U test. See also Supplementary Tables S4 and S7.

B) Correlation of original tumor consensus molecular subtype (CMS) with clinical and genetic features and niche factor requirements. Bubble plots show Spearman correlation (color key) and statistical significance (diameter: Fischer's exact test). Organoids with >1000 alterations (VAF >5%, observed in 3 of 30 lines) were defined as mismatch repair deficient (dMMR).

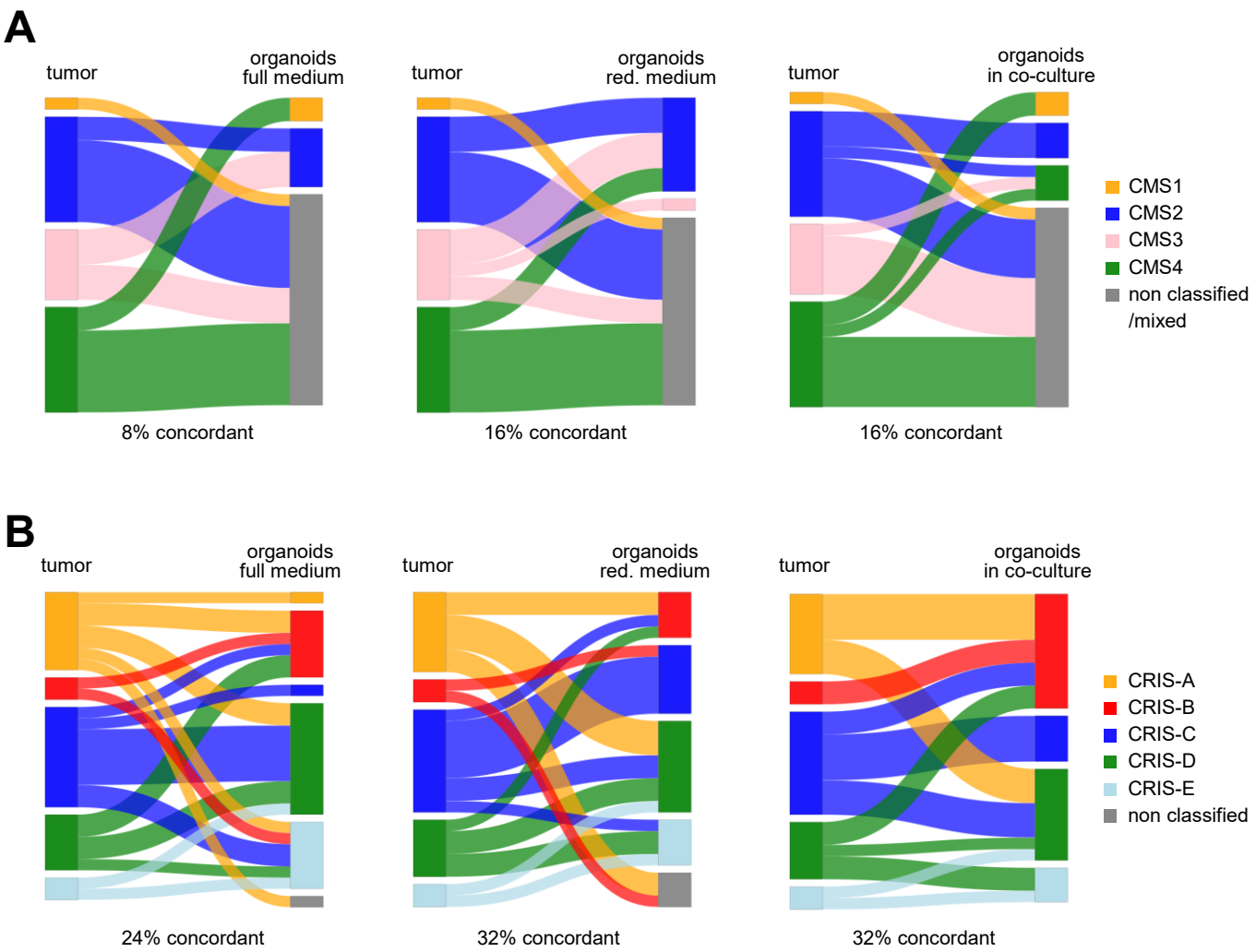

Supplementary Figure S8 | Influence of the stromal context on subtype classification of PDTOs. Sankey plots show CMS (A) and CRIS classification (B) of PDTOs in comparison to matched tumors under standard conditions (full medium; left), growth factor reduced medium (middle) and in transwell co-culture with CAFs (right). Classification was performed as described in the methods section in n=25 PDTOs using the RNA sequencing data shown in Fig. 4. Note that the concordance between the subtypes *in vitro* and matched tumors remains low also when analyzing PDTOs in co-culture with CAFs.

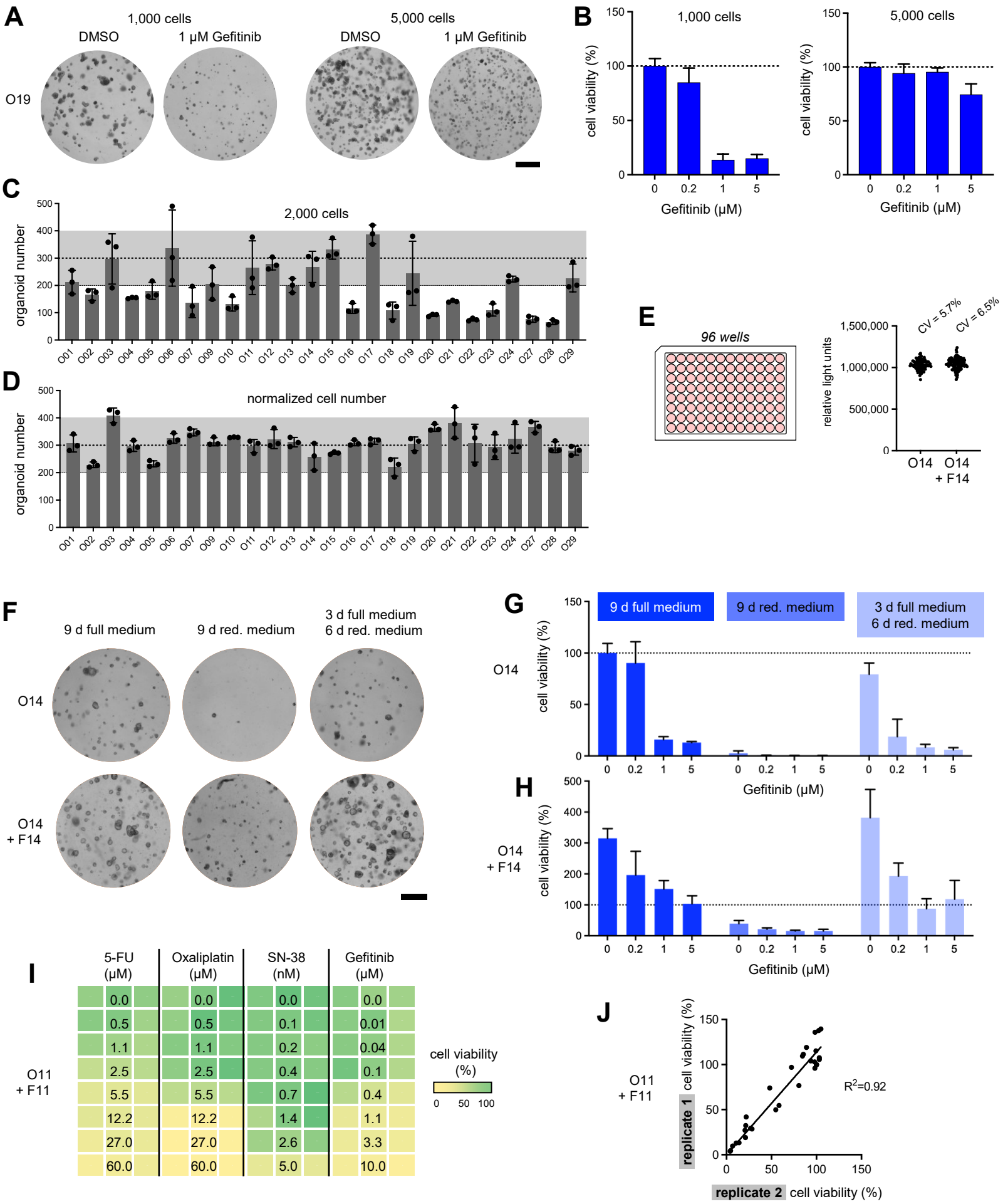

Supplementary Figure S9 | Development of a 3D platform to score the stromal influence on drug responses.

A-B) Seeding density affects drug response. Representative images 6 days after Gefitinib treatment (A) and measurement of cell viability by CellTiter-Glo® assay (B). Results were confirmed in 4 independent lines, each tested in triplicates.

C-D) Normalization of colony number to assure equal growth in all models. Colony number after seeding 2,000 cells (C) and adjusted colony number after normalized seeding (D). Colonies were counted using ImageJ software. Mean ±SD in triplicate wells. See Supplementary Table S7.

E) 96 well plate consistency in mono- and co-culture. Raw luminescence signals (untreated) and coefficient of variation (CV) are shown.

F-H) Optimized co-culture conditions. Cells were cultured in full medium, growth factor reduced medium, or first in full medium and then in reduced medium. Gefitinib was added after 3 days. Morphologic images of controls (F) and Gefitinib sensitivity (G, H) evaluated by luciferase measurement in technical triplicates.

I) Tumor cell viability in co-cultures in 96 well format. Heatmap of representative luciferase data in presence of 7 concentrations of 5-FU, Oxaliplatin, SN-38 and Gefitinib (each in triplicates).

J) Reproducibility of drug sensitivity data in co-culture format. Average cell viability between replicate plates (each in triplicates). All scale bars are 1 mm.

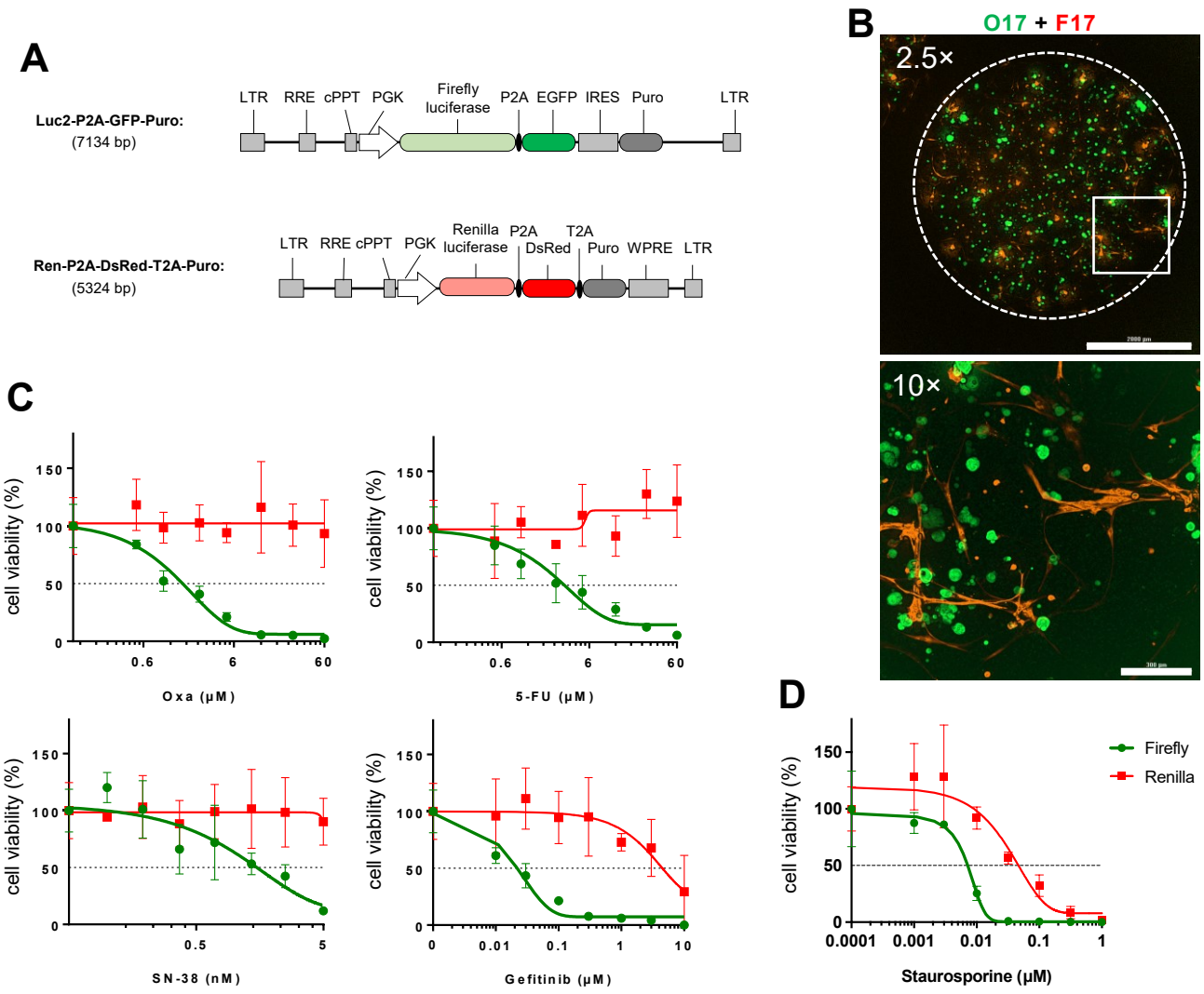

Figure S10 | Dual luciferase co-culture assay.

A) Lentiviral constructs to drive expression of Firefly luciferase (luc2)/EGFP or Renilla luciferase/DsRed (both separated by a P2A peptide). Stable expression is selectable by a puromycin resistance marker. Additional features are: long-terminal repeats (LTR), Rev response element (RRE), central polypurine tract (cPPT), phosphoglycerate kinase (PGK) promoter and the Woodchuck Hepatitis Virus Posttranscriptional Regulatory Element (WPRE).
B) Co-culture of CRC organoids (O17) and fibroblasts (F17) that were transduced to stably express Firefly luciferase/GFP and Renilla luciferase/DsRed, respectively. Co-culture was performed at a regular cell density and confocal image stacks of GFP and DsRed are shown at low (2.5×) and high (10×) magnification. The white circle shows Matrigel outlines, the white box shows magnified region. Scale bars are: 2000 µm and 300 µm.
C-D) Parallel dose-response in co-cultures by dual luciferase assay. Tumor organoids (O11) show increased sensitivity to 5-FU, Oxaliplatin, SN-38 and Gefitinib (C) compared to autologous CAFs (F11). Staurosporine (D) was used as a positive control targeting both compartments. Mean ±SD in triplicate wells.

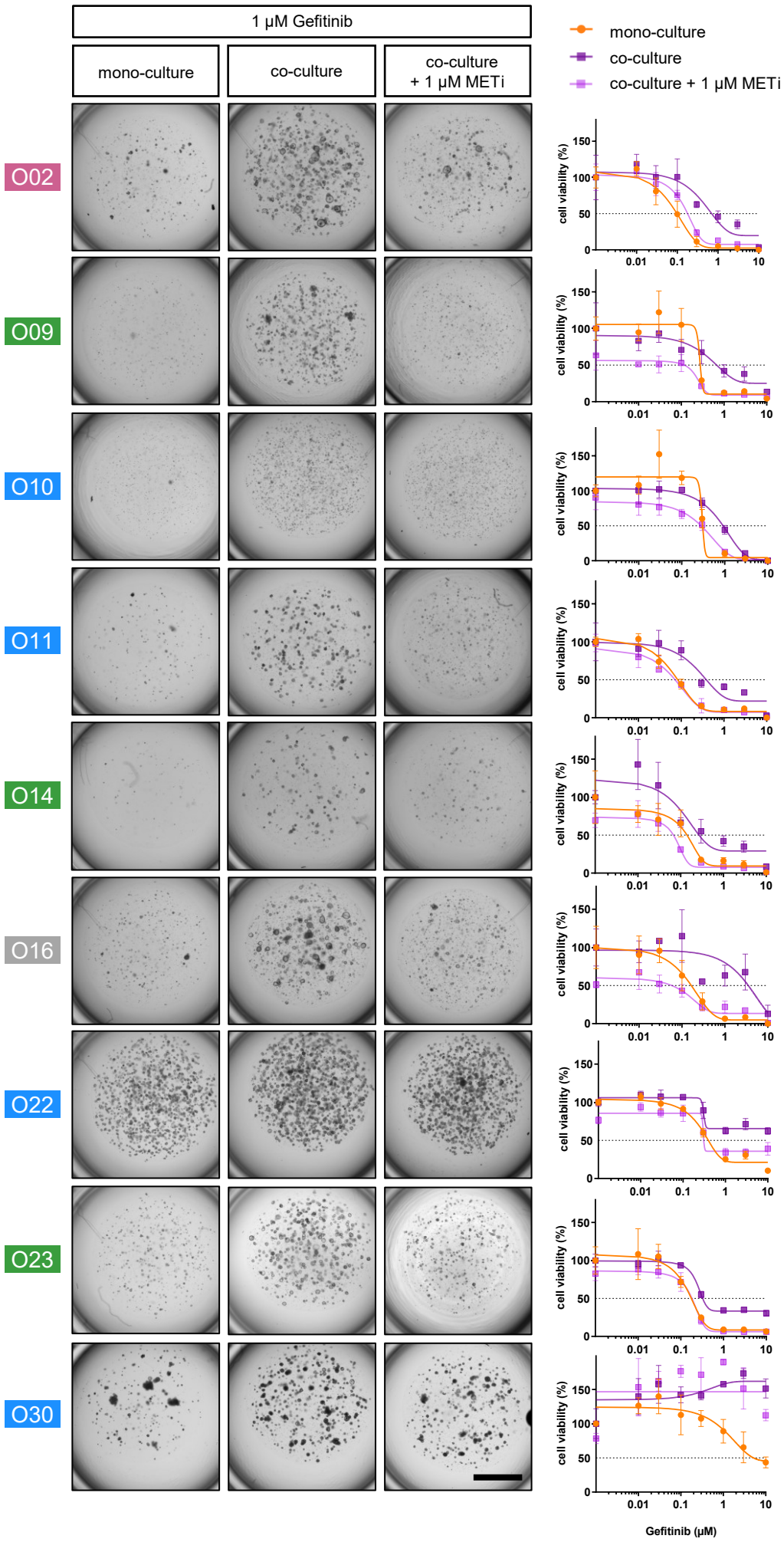

Supplementary Figure S11 | Validation of MET as a target to overcome stroma-induced Gefitinib resistance.
Representative images (2.5× left) and quantification of Gefitinib dose response (right) in CRC organoids (n=9). Images were captured after 6 days in presence of 1 µM Gefitinib in monoculture, CAF co-culture, or co-culture with 1 µM MET-inhibitor (BAY-474). Scale bar is 2000 µm. Tumor cell viability was determined by luciferase measurement. Experiments were performed as in Fig. 6A. Mean values ±SD in triplicate wells relative to DMSO after 6 days in presence of various concentrations of Gefitinib. Compared to mono-cultures (orange lines), Gefitinib resistance is observed in co-cultures (purple lines). Combined treatment with 1 µM BAY-474 (light purple lines) restores Gefitinib sensitivity in 8/9 co-cultures. Note that BAY-474 treatment did not potentiate Gefitinib sensitivity in mono-cultures (data not shown).

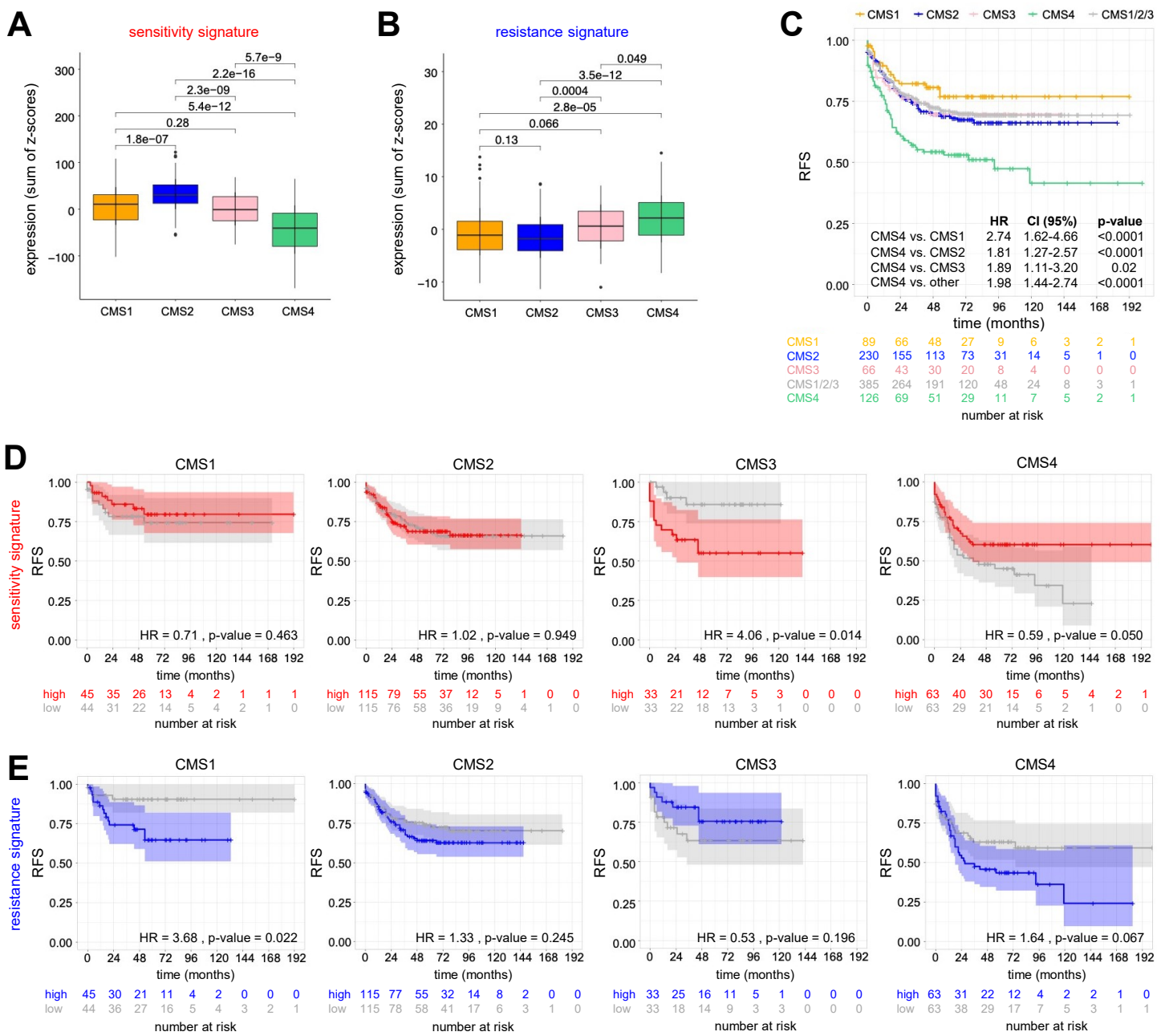

Supplementary Figure S12 | Comparison of co-culture derived drug signatures with CMS subtypes.

A-B) Expression of sensitivity (A) and resistance (B) signatures based on the *CAF drug influence* in public expression dataset GSE39582. Samples were grouped by CMS and for each sample, the sum of z-scores is shown as box plots. Statistical analysis by t-test, Bonferroni correction for multiple testing.

C-E) Kaplan-Meier analysis of relapse free survival (RFS; GSE39582). Comparison between subtypes (C) and subtype-specific analysis of sensitivity (D) and resistance signatures (E). Curves in (D, E) represent samples with high (red and blue) and low (grey) median expression. Shaded regions show confidence intervals. Hazard ratio and and p-values (univariate log-rank test) are marked.

CMS classification for all cases was reported in Guinney et al., 2015 (Synapse ID: 10.7303/syn2623706).